nature immunology

Tissue signals imprint ILC2 identity with anticipatory function

Roberto R. Ricardo-Gonzalez[1,8], Steven J. Van Dyken [2,7,8], Christoph Schneider[2], Jinwoo Lee [2], Jesse C. Nussbaum[2], Hong-Erh Liang[2], Dedeepya Vaka[3], Walter L. Eckalbar[2,4], Ari B. Molofsky[5], David J. Erle [2,4] and Richard M. Locksley [2,6]*

Group 2 innate lymphoid cells (ILC2s) are distributed systemically and produce type 2 cytokines in response to a variety of stimuli, including the epithelial cytokines interleukin (IL)-25, IL-33, and thymic stromal lymphopoietin (TSLP). Transcriptional profiling of ILC2s from different tissues, however, grouped ILC2s according to their tissue of origin, even in the setting of combined IL-25-, IL-33-receptor-, and TSLP-receptor-deficiency. Single-cell profiling confirmed a tissue-organizing transcriptome and identified ILC2 subsets expressing distinct activating receptors, including the major subset of skin ILC2s, which were activated preferentially by IL-18. Tissue ILC2 subsets were unaltered in number and expression in germ-free mice, suggesting that endogenous, tissue-derived signals drive the maturation of ILC2 subsets by controlling expression of distinct patterns of activating receptors, thus anticipating tissue-specific perturbations occurring later in life.

LC2s are defined by their ability to produce type 2 cytokines, in particular IL-5 and IL-13, by integrating inputs from multiple ligands, including cytokines, neuropeptides, and eicosanoids[1,2]. The epithelial cytokines IL-33, IL-25, and thymic stromal lympho-poietin (TSLP) are powerful ILC2 activating ligands, and mice deficient in these signaling pathways display substantial compromise in the capacity of mature lung ILC2s to generate type 2 cytokines in response to helminths and allergens[3–7]. Recent analyses of murine and human ILCs have indicated transcriptomic heterogeneity of ILC2s in tissues[8–10]; however, direct comparisons of ILC2s among normal resting tissues are limited and complicated by sorting strategies that rely on surface markers that are variably expressed by ILCs. Furthermore, functional characterizations of the signals that establish the homeostatic activation profiles of ILC2s across and within disparate tissues, particularly in skin, are lacking.

In this study, we combine analysis of mouse cytokine reporter alleles with RNA-sequencing approaches to comprehensively assess the constitutively function-marked populations of ILC2s present in resting bone marrow and peripheral tissues[11,12]. We further analyze germ-free mice and mice triple-deficient in IL-33, IL-25, and TSLP signaling to uncover key determinants of homeostatic effector cytokine function, which remains intact even in the absence of commensal microbiota, as assessed by the ILC2-defining cytokines IL-5 and IL-13. Notably, although IL-5+ ILC2s required IL-33, IL-25, and TSLP signaling for optimal homeostatic type 2 cytokine competency in a tissue-dependent manner, the transcriptomic signatures imprinted by each tissue in which ILC2s reside dictated their identity. Receptiveness to independent activating signals was segregated by tissue, as highlighted by skin ILC2s, which, like smaller ILC2 subsets in lung and bone marrow, expressed the IL-18 receptor and produced type 2 cytokines in response to IL-18.

In the absence of IL-18, this ILC2 subset was functionally impaired both in the steady-state and after inflammatory skin challenge. The expression of activating receptors by a tissue-specific program, even in the absence of ligand-receptor signals, reveals an anticipatory logic underpinning the roles for type 2 immune responses among different organs and tissues.

Results

Basal activation defines tissue-resident ILC2s. The epithelial cytokines IL-33, IL-25, and TSLP are important activating signals for ILC2s in homeostasis and in response to tissue injury. To assess the impact of combined TSLP, IL-33, and IL-25 deficiency on ILC2s under steady-state conditions, we analyzed ILC2s from multiple tissues in 8- to 12-week-old YRS mice. These mice express reporter alleles for arginase-1 (*Yarg*), IL-5 (*Red5*, also called *R5*), and IL-13 (*Smart13*, also called *S13* or *huCD4*), which are highly expressed among resting (YR[7,11,13]) and activated (S[14,15]) ILC2s; cells from YRS mice triple-deficient in TLSP receptor, IL-33 receptor, and IL-25 (TKO-YRS[7]; Fig. 1a) were collected and analyzed similarly (below). Among lineage-negative (Lin−) cells from YRS mice, we assessed R5+ ILC2s in the lung, gut (small intestine lamina propria), fat (perigonadal adipose tissue), and skin; the latter had diminished Yarg expression and variable expression of other common ILC2 surface markers. ILC2s from bone marrow expressed Yarg but were R5− (Fig. 1b and Supplementary Fig. 1). These findings are consistent with previous characterizations of these reporter alleles[11,13,16]. Although bone marrow ILC2s did not spontaneously express the *R5* or *Smart13* reporter alleles as in other tissues, stimulation with phorbol 12-myristate 13-acetate (PMA) and ionomycin resulted in robust IL-5 and IL-13 release and expression of cytokine reporter alleles in >90% of these cells, thereby confirming the identity of
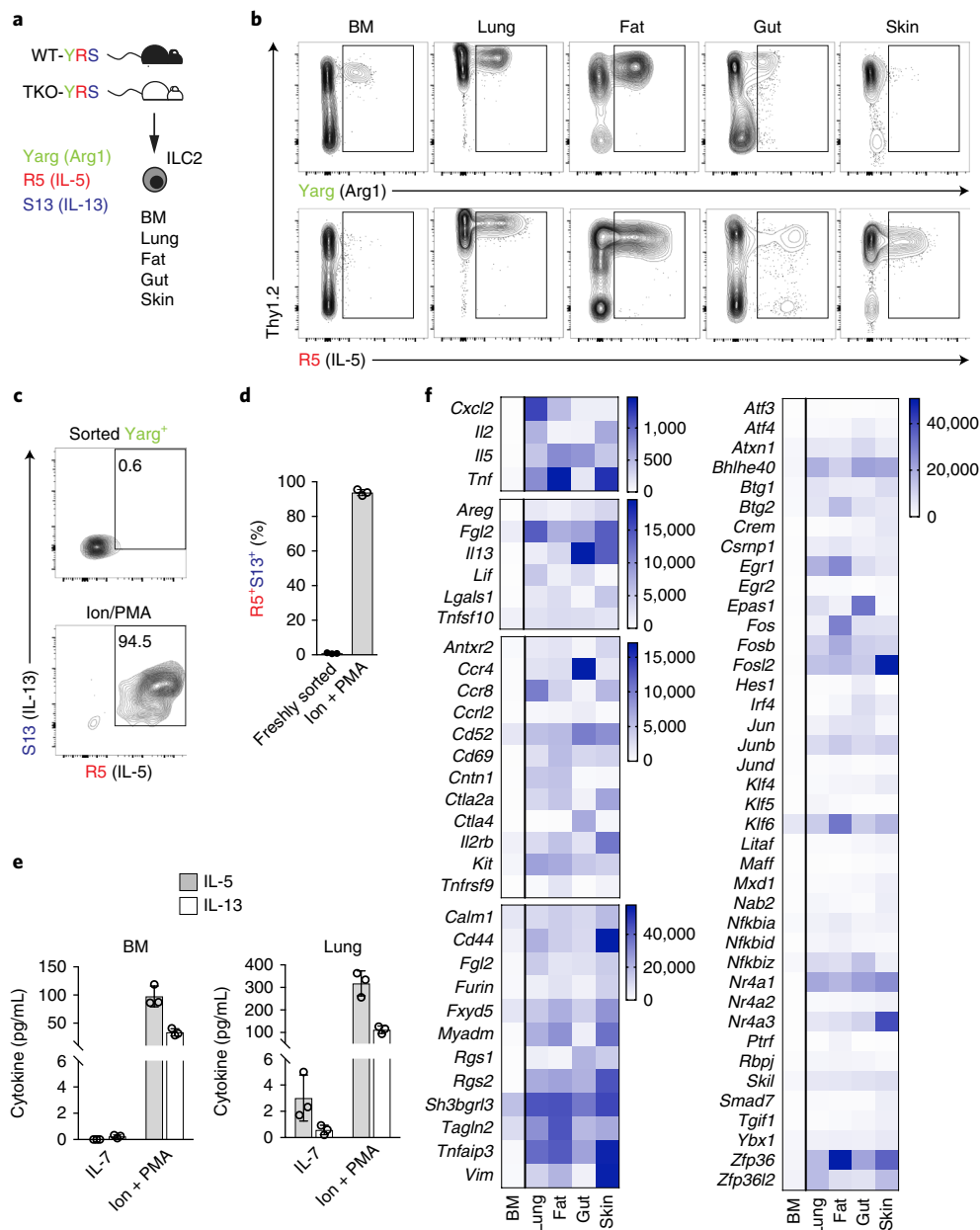
Fig. 1 | Steady-state ILC2 activation in multiple peripheral tissues. a, ILC2s were analyzed in multiple tissues from wild-type (WT) or $Crlf2^{-/-}IL25^{-/-}Il1rl1^{-/-}$ triple-deficient TKO-YRS mice. **b**, Representative flow cytometry of CD45$^+$Lin$^-$ cells from indicated WT-YRS mouse tissues. **c,d**, Representative flow cytometry (**c**) and percentage (**d**) of sorted Yarg$^+$ bone marrow (BM) ILC2 expressing $R5$ and $Smart13$ ($S13$) reporter alleles before and after stimulation with ionomycin (Ion) and PMA. **e**, IL-5 and IL-13 in supernatants of Yarg$^+$ ILC2 sorted from WT-YRS BM or lung tissue cultured in IL-7 or Ion + PMA for 24 h. **f**, RNA-seq analysis of select transcripts significantly enriched (false discovery rate (FDR) < 0.01) in R5$^+$ ILC2s from peripheral tissues (lung, gut, fat, skin) versus Yarg$^+$ BM ILC2s. Data in **b** and **c** are representative of 3 independent experiments and in **d**–**f** represent biological replicates ($n = 3$; mean ± s.d.).Data in **f** represent mean normalized read counts (fragments per million mapped reads) from biological replicates ($n = 3$, BM; $n = 5$, lung; $n = 6$, fat, gut, skin).

the Yarg$^+$ bone marrow ILC2 population by their ability to produce hallmark ILC2 cytokines (Fig. 1c–e).

The widespread distribution of R5$^+$ ILC2s in resting tissues suggested that ILC2s were activated by stimuli in the absence of apparent exogenous challenge. To decipher these signals, we performed RNA sequencing (RNA-seq) to compare the transcriptomes of purified R5$^+$ ILC2s isolated from lung, gut, fat, and skin against Yarg$^+$ ILC2s from bone marrow (which are R5$^-$). Compared to bone marrow ILC2s, peripheral tissue steady-state ILC2s expressed increased transcripts encoding growth factors, cytokines and cytokine-related

genes (for example, *Areg, Il2, Il5, Il13, Lif, Tnf, Tnfsf10*, and *Cish*), transcriptional regulators (for example, *Fos, Jun, Klf4, Klf5, Klf6, Irf4, Maff, Egr1, Egr2, Epas1*, and *Nfkbiz*), nuclear factors (for example, *Nr4a1, Nr4a2*, and *Nr4a3*), enzymes (for example, *Tnfaip3, Plk3, Clk4, Dusp1, Dusp4, Dusp5*, and *Dusp10*), and extracellular receptors associated with lymphoid cell activation (for example, *Cd44, Cd69, Il2rb, Ctla4, Kit, Ccr4*, and *Ccr8*; Fig. 1f, Supplementary Fig. 2, and Supplementary Table 1). These results highlight the basal activation state of tissue-resident ILC2s, although heterogeneity was apparent among different tissues. Indeed, the transcriptional profile
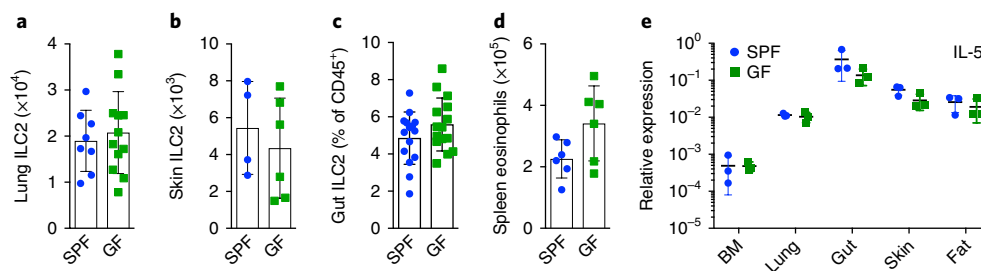
Fig. 2 | ILC2 distribution and homeostatic function is independent of the microbiota. a,b, Number of ILC2s (Lin⁻CD45⁺Thy1.2⁺CD25⁺) in lungs (**a**) and skin (**b**). **c,** Percentage of gut ILC2s (Lin⁻CD45⁺IL17rb⁺KLRG1⁺) of total CD45⁺ cells. **d,** Number of spleen eosinophils in C57BL/6 mice housed in SPF or germ-free (GF) conditions. **e,** Quantitative real-time PCR (qPCR) analysis of *Il5* transcript abundance among ILC2s sorted from SPF or GF mouse tissues. Data in **a–d** pooled from 2 or more independent experiments with $n \geq 4$ from each tissue and expressed as mean ± s.d. Data in **e** represent biological replicates ($n = 3$; mean ± s.d.) and are normalized to *Rps17*.

of steady-state tissue ILC2s resembled the shared transcriptional programs of tissue-effector ILC2s and CD4⁺ helper T cells (T_H2) cells elicited by type 2 immune stimulation[7,17].

Basal ILC2 activation is independent of microbiota. Steady-state stimulation by commensal microbes has been implicated in epigenetic and transcriptional alterations among intestinal ILC subsets[10]. With this in mind, we examined the tissue ILC2 activation program in germ-free mice as compared with mice housed in specific-pathogen-free (SPF) barrier conditions. Similar numbers of ILC2s (defined in lungs, skin, fat, and bone marrow as Lin⁻CD45⁺Thy1.2⁺CD25⁺, or in gut as Lin⁻CD45⁺KLRG1⁺IL-17Rb⁺, in the absence of the fluorescent reporters) were recovered from the lungs, skin, gut, fat, and bone marrow of germ-free and SPF mice (Fig. 2a–c and Supplementary Fig. 3a,b). Additionally, steady-state eosinophil numbers, which depend on ILC2-derived IL-5[11], were not significantly different in germ-free animals as compared to SPF controls ($P = 0.0661$; Fig. 2d), indicating that although the presence or absence of particular commensal microbes can alter intestinal ILC subset composition[10], these changes do not significantly impact cytokine-influenced functional outcomes of the tissue ILC2 activation program. In confirmation of these findings, we detected similar expression of *Il5* transcripts in comparing germ-free and SPF ILC2s isolated from bone marrow, fat, lung, gut, and skin (Fig. 2e). Transcriptional abundance for *Gata3* and *Arg1*, and for receptor components for tissue-derived cytokines, such as *Il1rl1* (encoding the IL-33 receptor subunit T1/ST2), *Il17rb* (encoding the IL-25 receptor subunit IL17RB), and *Tnfaip3* (encoding the ubiquitin-modifying enzyme A20 induced by nuclear factor kappa-light-chain-enhancer of activated B cells (NF-κB) signaling), were also comparable (Supplementary Fig. 3c–g). Thus, tissue programs driving peripheral ILC2 activation are independent of commensal microbes and are likely driven by tissue-intrinsic signals.

Distinct tissue signals drive resident ILC2 activation. Tissue-derived signals, such as the cytokines IL-25, IL-33, and TSLP, control type 2 cytokine production from ILC2s in peripheral tissues in response to infectious or homeostatic perturbations[3,7,15,18,19], and they synergize with other ILC2 activation signals such as leukotrienes[20] and neuropeptides[21]. We assessed whether these three signals contributed to the resting activation profile of ILC2s by examining multiple tissues from triple-reporter YRS and TKO-YRS mice, which lack responsiveness to TLSP, IL-33, and IL-25 cytokine signals. Notably, TKO-YRS mice harbored normal numbers of total ILC2s in lung, fat, and gut (lung, $P = 0.1024$; fat, $P = 0.6638$; gut, $P = 0.0636$; Fig. 3a–c), although the numbers of activated IL-5-expressing R5⁺ ILC2s were significantly reduced in these peripheral tissues (lung $P = 1.6244 \times 10^{-7}$; fat, $P = 0.0009$; gut, $P = 6.0366 \times 10^{-18}$;
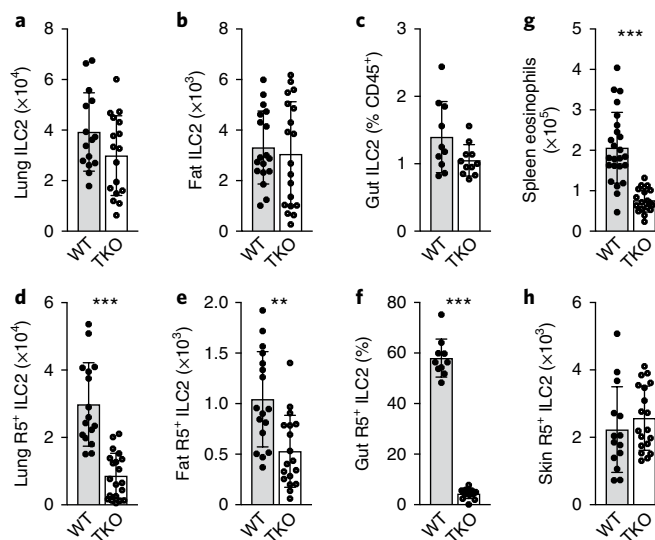

Fig. 3 | Tissue-resident ILC2s depend on distinct tissue signals. **a,b,** Number of ILC2s (Lin⁻CD45⁺Thy1.2⁺CD25⁺) in lungs (**a**) and fat (**b**). **c,** percentage of ILC2s (Lin⁻CD45⁺KLRG1⁺) of total CD45⁺ cells in gut among WT- or *Crlf2⁻/⁻Il25⁻/⁻Il1rl1⁻/⁻*TKO-YRS backgrounds. **d–f,** Number of R5⁺ ILC2s (Lin⁻CD45⁺) in lungs (**d**), fat (**e**), and gut (**f**) tissues of WT-YRS and TKO-YRS mice. **g,** Numbers of eosinophils in spleen. **h,** Number of R5⁺ ILC2s in skin (Lin⁻CD45⁺) of WT-YRS and TKO-YRS mice. Data pooled from 2 or more independent experiments with $n \geq 10$ mice per group, represented as mean ± s.d.; **$P < 0.001$, ***$P < 0.0001$.

Fig. 3d–f and Supplementary Fig. 4), extending prior observations of lung ILC2s[7]. Peripheral eosinophil numbers were also diminished in TKO-YRS mice, consistent with the role for ILC2s in sustaining systemic IL-5 (Fig. 3g). The magnitude of the reduction in R5⁺ ILC2s, however, was not consistent among peripheral tissues; notably, the skin contained comparable numbers of R5⁺ ILC2s in wild-type YRS and in TKO-YRS mice (Fig. 3h), indicating that signals other than IL-25, IL-33, and TSLP sustain steady-state IL-5 production from skin ILC2s.

To explore this further, we compared the transcriptional profiles of ILC2s from YRS and TKO-YRS mice isolated from multiple tissues. In agreement with the reporter gene expression and in agreement with prior studies[7,15,19], type 2 cytokine transcripts were reduced in TKO-YRS ILC2s isolated from lung, fat, and gut (Supplementary Fig. 5d,e). Clustering based on the top 1,000 differentially expressed genes, however, revealed that the major transcriptional signatures
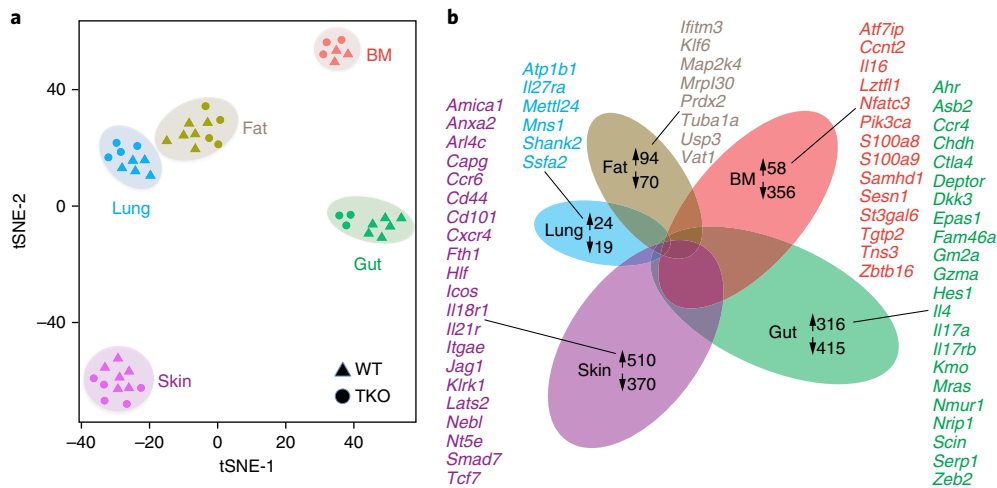
Fig. 4 | Transcriptional heterogeneity of tissue-resident ILC2s. a, t-Distributed stochastic neighbor embedding (tSNE) plot representing ILC2 samples. ILC2s were sorted from lung, fat, gut, skin (Lin⁻CD45⁺Red5⁺), and bone marrow (BM, Lin⁻CD45⁺Yarg⁺) as outlined in the gating strategy shown in Supplementary Fig. 1. **b,** RNA-seq analysis of differentially expressed transcripts (FDR < 0.01) among ILC2s from each tissue vs. all other tissues; select upregulated transcripts in each tissue highlighted. Data pooled from 3 independent experiments with n ≥ 3 biological replicates per group. Numbers with arrows indicate numbers of transcripts upregulated or downregulated.
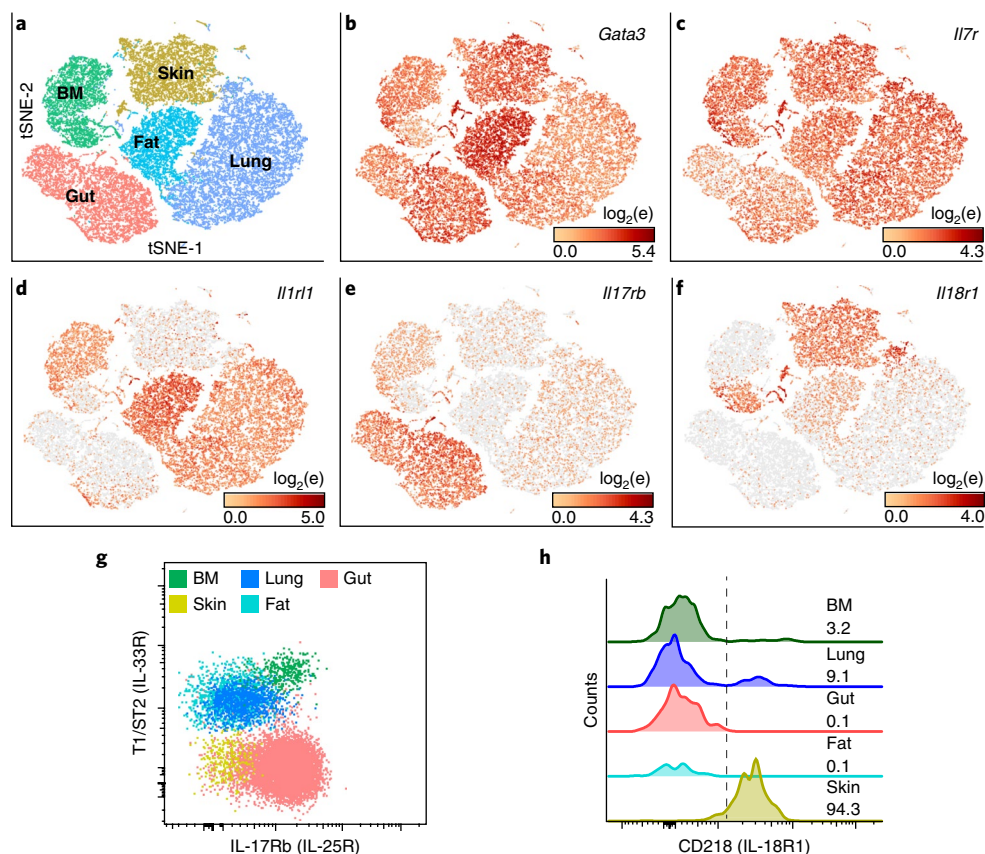

Fig. 5 | Tissue map of ILC2 signals revealed by scRNA-seq. a, tSNE plot representing 35,396 ILC2s sorted from BM (Lin⁻CD45⁺Yarg⁺), lung, fat, gut, and skin (Lin⁻CD45⁺Red5⁺) analyzed by scRNA-seq. **b–f,** Normalized relative expression of *Gata3* (**b**), *Il7r* (**c**), *Il1rl1* (**d**), *Il17rb* (**e**), and *Il18r1* (**f**) transcripts. **g,h,** Representative flow cytometric staining for T1/ST2 (IL-33R), IL17Rb (IL-25R) (**g**), and CD218 (IL-18R1) (**h**) among ILC2s from indicated WT-YRS mouse tissues. Data in **g** and **h** are representative of 3 independent experiments; numbers in **h** represent the percentages of ILC2s positive for CD218 (right of dotted line).

from wild-type and TKO ILC2s were tissue-specific and independent of the presence or absence of these epithelial cytokines (Fig. 4a and Supplementary Fig. 5a–e). Among wild-type R5⁺ or Yarg⁺ ILC2s, tens to hundreds of transcripts were differentially expressed

by ILC2s collected from single tissues as compared to all other tissues, with gut and skin ILC2s showing the greatest numbers of divergent transcripts from the other groups. Notably, we observed enhanced *Il17rb* expression in gut ILC2s but substantially increased
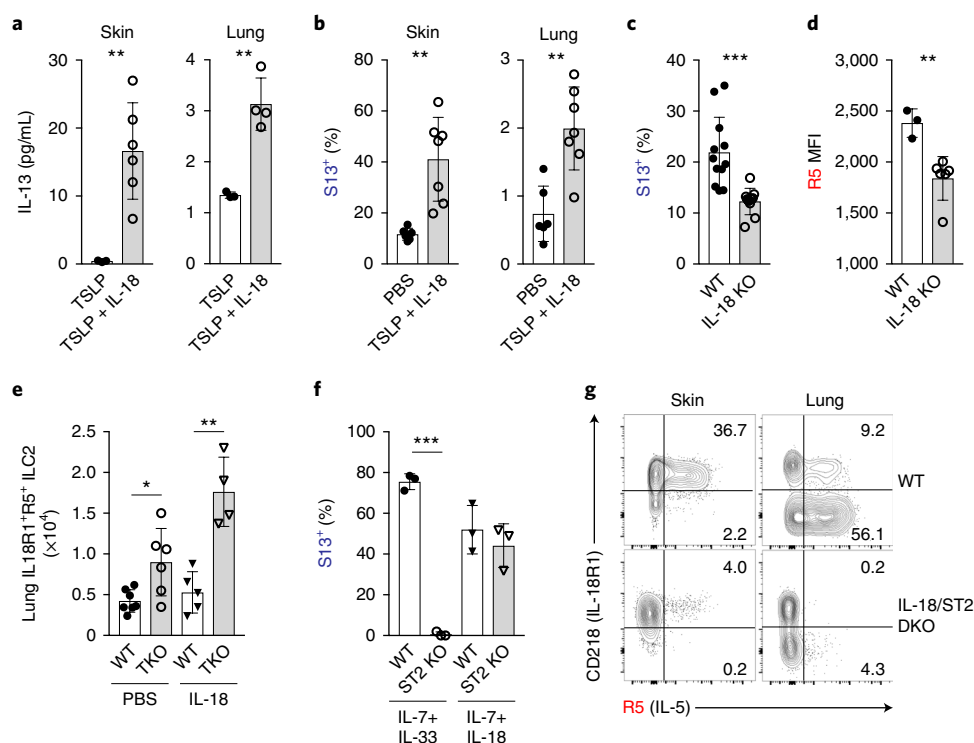
Fig. 6 | IL-18 independently mediates ILC2 subset activation. a, IL-13 in supernatants of ILC2s (Lin⁻CD45⁺Thy1.2⁺Red5⁺) sorted from skin or lung tissue and cultured in TSLP alone or TSLP and IL-18. **b**, Percentage of skin and lung ILC2s (Lin⁻CD45⁺Thy1.2⁺Red5⁺) expressing *S13* reporter allele after intradermal injection of phosphate-buffered saline (PBS) or TSLP and IL-18. **c,d**, Percentage of skin ILC2s expressing *S13* reporter allele (**c**) and R5 reporter median fluorescence intensity (MFI) (**d**) among skin ILC2s from WT and IL18-deficient (KO) mice on a R5; Smart13 dual-reporter background. **e**, Number of IL-18R1⁺R5⁺ ILC2s in lungs of WT-YRS and TKO-YRS mice 24 h after intranasal administration of PBS or recombinant IL-18. **f**, Percentage of IL-18R1⁺Yarg⁺ ILC2s sorted from BM of WT or ST2 KO mice expressing *S13* reporter allele 24 h after culture in IL-7+IL-33 or IL-7+IL-18. **g**, Representative flow cytometry of R5 reporter expression among skin and lung ILC2s (Lin⁻CD45⁺Thy1.2⁺) from WT and IL-18⁻/⁻ST2⁻/⁻-deficient (DKO) mice on an R5;S13 dual-reporter background. Numbers indicate percent R5⁺ in each quadrant. Data in **a–f** pooled from 2 or more independent experiments for a total of at least 3 mice per group, represented as mean ± s.d.; *P < 0.05, **P < 0.01, ***P < 0.001.

Il18r1 expression in skin ILC2s (Fig. 4b, Supplementary Fig. 5f,g, and Supplementary Table 1). Collectively, these findings suggest that distinct tissue-derived factors contribute to ILC2 subset activation in the steady state.

Single-cell RNA-sequencing distinguishes ILC2 subsets. To explore further the nature of ILC2 tissue signatures and to discern whether these differences identified by bulk RNA-seq resulted from contamination by nonhematopoietic tissue cells, we performed single-cell RNA-sequencing (scRNA-seq) on 35,396 sorted ILC2s from bone marrow and peripheral tissues. In confirmation of the bulk sequencing results, scRNA-seq analysis of the aggregated ILC2s from multiple tissues showed segregation by tissue, which could be further subclustered within each tissue, revealing novel intratissue ILC2 subsets (Fig. 5a and Supplementary Fig. 6a–c). We observed minimal (<2%; Supplementary Fig. 6b) contamination by non-ILC2 cells, and, in agreement with the bulk sequencing results, common transcripts such as *Gata3*, *Il7r*, and *Crlf2* (encoding the TSLP receptor subunit TSLPR) were expressed by the majority of ILC2s across tissues, whereas other transcripts were enriched in particular tissues (Fig. 5b–f and Supplementary Figs. 6c and 7), consistent with tissue-specific functional roles. *Il1rl1*, encoding an IL-33 receptor subunit, was enriched among fat and lung ILC2s, corresponding to a loss of IL-5 reporter R5 expression in ILC2s from these tissues in mice lacking this receptor (Fig. 5d and Supplementary Fig. 4). The gene encoding IL-25R, *Il17rb*, was abundant among gut ILC2s and matched the loss of R5 expression predominantly seen among small-intestinal ILC2s in mice lacking IL-25 (Fig. 5e and Supplementary

Fig. 4). These findings are consistent with prior studies linking IL-33 to steady-state ILC2 function in fat and lung[19,22] and IL-25 to small-intestinal ILC2 function[15,23]. In contrast, skin ILC2s showed comparatively low expression of both IL-25 and IL-33 receptors, as assessed both by flow cytometry and transcript analysis, and consistent with unaltered IL-5 expression among TKO skin ILC2s (Fig. 5d,e,g, Supplementary Figs. 4 and 6c, and Supplementary Table 1). Of note, skin ILC2s expressed IL-18R1 (CD218) cell surface protein and *Il18r1* transcripts, even in germ-free mice (Supplementary Fig. 3h). In agreement with the bulk RNA-seq results, IL-18 receptor subunit expression was also enriched in subsets of lung and bone marrow ILC2s identified by scRNA-seq and flow cytometry (Fig. 5f,h and Supplementary Fig. 6b,c). These findings raise the possibility that IL-18 could influence ILC2 function in a tissue- and subset-specific manner.

IL-18 independently activates IL-18 receptor-bearing ILC2s. IL-1 cytokine family members, including IL-18 and IL-33, can induce cytokine expression from lymphoid cells, particularly in the presence of STAT5 activators such as IL-7 and TSLP[24,25]. To test the function of IL-18 on these IL-18R-bearing peripheral ILC2 subsets, we sorted ILC2s from skin and lung and cultured them with IL-18 and TSLP in vitro. Compared to TSLP alone, ILC2s produced significantly higher amounts of IL-13 in the presence of IL-18 (skin, P = 0.0066; lung P = 0.0021; Fig. 6a), in agreement with a recent characterization of IL-18-responsive ILCs isolated from human tissues[9]. Intradermal injection of IL-18 and TSLP into S13 reporter mice increased IL-13 reporter expression among both skin and
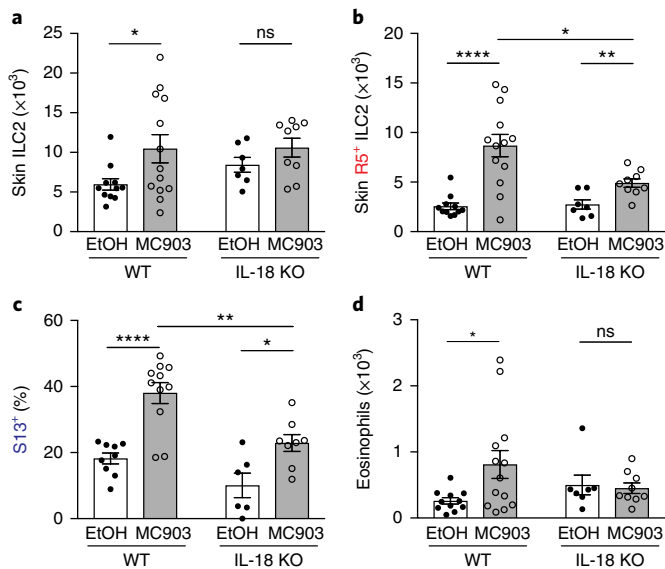
Fig. 7 | Blunted type 2 skin inflammation in the absence of IL-18.
a–d, Total skin ILC2s (Lin⁻CD45⁺Thy1.2⁺CD25⁺) (**a**), R5⁺ ILC2s (Lin⁻CD45⁺Thy1.2⁺Red5⁺) (**b**), percentage of R5⁺ ILC2s expressing *S13* reporter allele (**c**), and total eosinophils (**d**) in ears of wild type or IL-18 KO mice treated with ethanol (EtOH) or MC903. Data pooled from 2 or 3 individual experiments with $n \geq 6$ for each experimental group and are represented as mean ± s.e.m.; *$P < 0.05$; **$P < 0.005$; ***$P < 0.0005$; ****$P < 0.0001$.

lung ILC2s (Fig. 6b), indicating that IL-18R1 expression on ILC2s mediates type 2 cytokine production from these cells in response to IL-18. To determine whether IL-18 contributes to the steady-state production of type 2 cytokines from ILC2s, we compared *Smart13* and *R5* reporter allele expression on wild-type ILC2s to those on an IL-18-deficient background (IL-18 knockout). Although the numbers of R5⁺ ILC2s in wild-type and IL-18 knockout mice were comparable (Supplementary Fig. 8a,b), *Smart13* expression and R5 fluorescence were significantly reduced in IL-18-deficient skin ILC2s in comparison with wild-type control cells (*Smart13, $P = 0.000472$;* R5. $P = 0.00570$; Fig. 6c,d), revealing a nonredundant role for IL-18 as a steady-state activator of IL-18R1-expressing ILC2s. We considered how IL-18 might contribute to steady-state activation of ILC2s in the presence or absence of other endogenous activating cytokines, including IL-25 and IL-33, in light of their tissue- and subset-specific receptor expression patterns. Although total R5⁺ ILC2s were reduced in the lungs of TKO animals (Fig. 3d and Supplementary Fig. 4), the IL-18R1⁺R5⁺ ILC2 subset was expanded in number when compared to wild-type control mice, both in the steady-state and in response to intranasal IL-18 (Fig. 6e). These observations indicate that IL-18 could preferentially mediate activation and type 2 cytokine production from the IL-18R1-expressing ILC2 subset independent of IL-25, IL-33, and TSLP. In further support of this notion, IL-18 mediated activation and cytokine reporter expression among bone marrow IL-18R1⁺Yarg⁺ ILC2s in the absence of IL-33R (ST2) expression, although the latter was required to respond to IL-33 (Fig. 6f). As receptor components for both IL-33 and IL-18 were expressed on some ILC2 subsets, we tested whether these two cytokines combined to control the steady-state expression of IL-5 in IL-18R1-expressing ILC2 subsets in skin and lung. Indeed, R5 expression among lung and skin ILC2 subsets bearing CD218 and/or ST2 was substantially reduced in mice that lacked both IL-18 and the IL-33 receptor ST2 when compared to wild-type controls (Fig. 6g). Thus, patterns of activating receptors have biologic significance that are organ-specific and based upon the subsets of ILC2s populating that tissue.

Blunted type 2 skin inflammation in the absence of IL-18. ILC2s have been shown to be increased in lesional skin of patients with atopic dermatitis and in mouse models of atopic dermatitis-like inflammation[5,26]. Our findings that IL-18 activated skin ILC2s and that loss of IL-18 led to reduced activation of skin ILC2s in homeostasis (Fig. 6a–d) led us to further examine whether IL-18 contributed to ILC2 function in the context of an in vivo mouse model of skin inflammation. To test this, we used topical application of MC903, a well-characterized mouse model of atopic-like inflammation that has been shown to activate ILC2s and cause eosinophilia, skin swelling, and type 2 inflammation[26]. Compared to wild-type mice, IL-18-deficient mice exhibited decreased skin tissue accumulation of total ILC2s and of IL-5- and IL-13-producing ILC2s (Fig. 7a–c), which are critical determinants of eosinophil recruitment into tissues[7]. Indeed, mice deficient in IL-18 also showed a corresponding decrease in the numbers of eosinophils recruited to ear skin tissue in response to MC903 (Fig. 7d). These data suggest that IL-18 not only influences basal ILC2 subset activation in the steady-state but also contributes to its function in models of atopic dermatitis.

Discussion

ILC2s are largely tissue-resident cells with a canonical effector function centered on the production of type 2 cytokines, particularly in response to key activating cytokines like IL-33, IL-25, and TSLP. Here we show that expression of these cytokine receptors impacts cytokine discharge from ILC2s, but with varying effects in different tissues, reflecting diversity in receptor expression on ILC2 subsets in different organs. Indeed, some ILC2 subsets, including most skin ILC2s, express low levels of receptors for epithelial cytokines IL-33, IL-25, and TSLP; instead they are activated dominantly by IL-18, which is highly expressed in skin ILC2s and in subpopulations of ILC2s in lung and bone marrow. Strikingly, transcriptomic profiling of ILC2s revealed tissue-specific subsets of cells whose expression patterns remained largely unaffected by the absence of signaling through the three canonical epithelial cytokines. These tissue-specific expression patterns, including the capacity to respond to epithelial cytokines or IL-18, were normal in germ-free and cytokine-deficient mice, uncovering a tissue-derived signature responsible for preemptively establishing responsiveness of ILC2 subsets in different tissues in an anticipatory fashion, since normal receptor expression and tissue distribution occurred even in the absence of ligand-mediated stimulation.

These tissue signatures reveal new potential therapeutic targets among particular cytokine receptor-bearing subsets of ILC2s. Notably, in IL-18-deficient mice, the IL-18R-bearing ILC2s in the skin exhibited a substantial defect in the homeostatic activation of ILC2s in vivo. Moreover, ILC2 proliferation and activation, as well as eosinophil recruitment, were blunted in IL-18-deficient animals after skin challenge with MC903, a well-characterized mouse model of atopic-like dermatitis. These results are particularly noteworthy, as transgenic mice that overexpress IL-18 in keratinocytes develop severe dermatitis[27], and elevated IL-18 correlates with disease severity in atopic dermatitis[28,29], raising the possibility that targeting IL-18 may represent a means to ameliorate type 2 immune activation in the skin. In addition, given that receptor components for both IL-33 and IL-18 were expressed on some ILC2 subsets, activation by these two signals either alone or in combination may influence allergic diseases like asthma and atopic dermatitis. Indeed, the genes for IL-18R1 and IL-33R receptors are located together in the genome at an interval linked by genome-wide association studies with risk for allergic diseases in large cohorts[30,31].

Further study using appropriate fate-mapping tools will be required to determine whether these tissue-specific expression profiles are acquired during fetal or perinatal development when ILC2s become established in tissues[12,16,32], and how these programs

are engaged during differentiation from bone marrow precursors in adults, or after tissue insults like helminths and allergens. Strikingly, ILC2 effector function is expressed postbirth and may create an additional layer of control along with tissue-resident macrophages during this critical period of growth and development, in which cell identity becomes established in temporal proximity to tissue differentiation[33], and before the maturation of tissue-resident adaptive immunity. Notably, our findings suggest discrete stages in the development of mature tissue ILC2s[34]. ILC2 precursors are first seeded into tissues, where they acquire a tissue-specific transcriptome characterized by expression of distinct subsets of activating receptors and an activated, poised phenotype. The subsequent generation of the canonical type 2 cytokines is then regulated by the generation of distinct sets of ligands that converge on receptors expressed by ILC2s specific to that tissue. How and why these diverse tissue pathways converge on the canonical type 2 cytokines and related effectors in ILC2s distributed across multiple tissues continues to be an important issue that may provide understanding of processes firmly at the nexus of homeostasis and allergic immunity.

Methods

Any methods, additional references, Nature Research reporting summaries, source data, statements of data availability and associated accession codes are available at https://doi.org/10.1038/s41590-018-0201-4.

References

1. Moltke, von, J. & Locksley, R. M. I-L-C-2 it: type 2 immunity and group 2 innate lymphoid cells in homeostasis. *Curr. Opin. Immunol.* **31**, 58–65 (2014).
2. Klose, C. S. N. & Artis, D. Innate lymphoid cells as regulators of immunity, inflammation and tissue homeostasis. *Nat. Immunol.* **17**, 765–774 (2016).
3. Neill, D. R. et al. Nuocytes represent a new innate effector leukocyte that mediates type-2 immunity. *Nature* **464**, 1367–1370 (2010).
4. Klein Wolterink, R. G. J. et al. Pulmonary innate lymphoid cells are major producers of IL-5 and IL-13 in murine models of allergic asthma. *Eur. J. Immunol.* **42**, 1106–1116 (2012).
5. Salimi, M. et al. A role for IL-25 and IL-33-driven type-2 innate lymphoid cells in atopic dermatitis. *J. Exp. Med.* **210**, 2939–2950 (2013).
6. Licona-Limón, P., Kim, L. K., Palm, N. W. & Flavell, R. A. TH2, allergy and group 2 innate lymphoid cells. *Nat. Immunol.* **14**, 536–542 (2013).
7. Van Dyken, S. J. et al. A tissue checkpoint regulates type 2 immunity. *Nat. Immunol.* **17**, 1381–1387 (2016).
8. Robinette, M. L. et al. Transcriptional programs define molecular characteristics of innate lymphoid cell classes and subsets. *Nat. Immunol.* **16**, 306–317 (2015).
9. Simoni, Y. et al. Human Innate Lymphoid Cell Subsets Possess Tissue-Type Based Heterogeneity in Phenotype and Frequency. *Immunity* **46**, 148–161 (2017).
10. Gury-BenAri, M. et al. The Spectrum and Regulatory Landscape of Intestinal Innate Lymphoid Cells Are Shaped by the Microbiome. *Cell* **166**, 1231–1246.e13 (2016).
11. Nussbaum, J. C. et al. Type 2 innate lymphoid cells control eosinophil homeostasis. *Nature* **502**, 245–248 (2013).
12. Huang, Y. et al. S1P-dependent interorgan trafficking of group 2 innate lymphoid cells supports host defense. *Science* **359**, 114–119 (2018).
13. Bando, J. K., Nussbaum, J. C., Liang, H.-E. & Locksley, R. M. Type 2 innate lymphoid cells constitutively express arginase-I in the naive and inflamed lung. *J. Leukoc. Biol.* **94**, 877–884 (2013).
14. Liang, H.-E. et al. Divergent expression patterns of IL-4 and IL-13 define unique functions in allergic immunity. *Nat. Immunol.* **13**, 58–66 (2011).
15. Moltke, von, J., Ji, M., Liang, H.-E. & Locksley, R. M. Tuft-cell-derived IL-25 regulates an intestinal ILC2-epithelial response circuit. *Nature* **529**, 221–225 (2016).
16. Bando, J. K., Liang, H.-E. & Locksley, R. M. Identification and distribution of developing innate lymphoid cells in the fetal mouse intestine. *Nat. Immunol.* **16**, 153–160 (2015).
17. Shih, H.-Y. et al. Developmental Acquisition of Regulomes Underlies Innate Lymphoid Cell Functionality. *Cell* **165**, 1120–1133 (2016).
18. Van Dyken, S. J. et al. Chitin activates parallel immune modules that direct distinct inflammatory responses via innate lymphoid type 2 and γδ T cells. *Immunity* **40**, 414–424 (2014).
19. Molofsky, A. B. et al. Interleukin-33 and Interferon-γ Counter-Regulate Group 2 Innate Lymphoid Cell Activation during Immune Perturbation. *Immunity* **43**, 161–174 (2015).
20. Moltke, von, J. et al. Leukotrienes provide an NFAT-dependent signal that synergizes with IL-33 to activate ILC2s. *J. Exp. Med.* **214**, 27–37 (2017).
21. Cardoso, V. et al. Neuronal regulation of type 2 innate lymphoid cells via neuromedin U. *Nature* **549**, 277–281 (2017).
22. Saluzzo, S. et al. First-Breath-Induced Type 2 Pathways Shape the Lung Immune Environment. *Cell Rep.* **18**, 1893–1905 (2017).
23. Schneider, C. et al. A Metabolite-Triggered Tuft Cell-ILC2 Circuit Drives Small Intestinal Remodeling. *Cell* **174**, 271–284.e14 (2018).
24. Guo, L., Junttila, I. S. & Paul, W. E. Cytokine-induced cytokine production by conventional and innate lymphoid cells. *Trends Immunol.* **33**, 598–606 (2012).
25. Mohapatra, A. et al. Group 2 innate lymphoid cells utilize the IRF4-IL-9 module to coordinate epithelial cell maintenance of lung homeostasis. *Mucosal Immunol.* **9**, 275–286 (2016).
26. Kim, B. S. et al. TSLP elicits IL-33-independent innate lymphoid cell responses to promote skin inflammation. *Sci. Transl. Med.* **5**, 170ra16–170ra16 (2013).
27. Konishi, H. et al. IL-18 contributes to the spontaneous development of atopic dermatitis-like inflammatory skin lesion independently of IgE/stat6 under specific pathogen-free conditions. *Proc. Natl Acad. Sci. USA* **99**, 11340–11345 (2002).
28. Thijs, J. et al. Biomarkers for atopic dermatitis: a systematic review and meta-analysis. *Curr. Opin. Allergy Clin. Immunol.* **15**, 453–460 (2015).
29. Zedan, K. et al. Immunoglobulin e, interleukin-18 and interleukin-12 in patients with atopic dermatitis: correlation with disease activity. *J. Clin. Diagn. Res.* **9**, WC01–WC05 (2015).
30. Ferreira, M. A. et al. Shared genetic origin of asthma, hay fever and eczema elucidates allergic disease biology. *Nature Genet.* **49**, 1752–1757 (2017).
31. Demenais, F. et al. Multiancestry association study identifies new asthma risk loci that colocalize with immune-cell enhancer marks. *Nature Genet.* **50**, 42–53 (2018).
32. Steer, C. A. et al. Group 2 innate lymphoid cell activation in the neonatal lung drives type 2 immunity and allergen sensitization. *J. Allergy Clin. Immunol.* **140**, 593–595.e3 (2017).
33. Mass, E. et al. Specification of tissue-resident macrophages during organogenesis. *Science* **353**, aaf4238–aaf4238 (2016).
34. Kotas, M. E. & Locksley, R. M. Why Innate Lymphoid Cells? *Immunity* **48**, 1081–1090 (2018).

Author contributions

R.R.R.-G. and S.J.V.D. designed and performed experiments, analyzed and interpreted the data, and wrote the manuscript. C.S., J.L., J.C.N., H.-E.L., and A.B.M. contributed to experiments. D.V. analyzed scRNA-seq data, and W.L.E. and D.J.E. provided RNA-seq data analysis and expertise. R.M.L. directed the studies and wrote the manuscript with R.R.R.-G. and S.J.V.D.

Competing interests

The authors declare no competing interests.

Additional information

Supplementary information is available for this paper at https://doi.org/10.1038/s41590-018-0201-4.

Reprints and permissions information is available at www.nature.com/reprints.

Correspondence and requests for materials should be addressed to R.M.L.

Publisher's note: Springer Nature remains neutral with regard to jurisdictional claims in published maps and institutional affiliations.

Methods

Mice. Mice expressing *Il5*[Red5], *Arg1*[Yarg], and *Il13*[Smart] reporter alleles on wild-type and triple-deficient *Crlf2*^{−/−}*Il25*^{−/−}*Il1rl1*^{−/−} C57BL/6 J backgrounds were bred and maintained as described previously[7,9,10,28]. *Il18*^{−/−} mice were obtained from The Jackson Laboratory (Stock 004130) and crossed with mice expressing *Il5*[Red5] and *Il13*[Smart] alleles to generate *Il18*^{−/−} dual reporter mice. For all experiments, age-matched (7–14 weeks) and sex-matched mice maintained under specific pathogen-free conditions were used. For in vivo cytokine treatments, mice were injected subcutaneously with rmIL-18 (2.5 μg), rmTSLP (500 ng) in calcium- and magnesium-free phosphate buffered saline (PBS) or intranasally with rmIL-18 (500 ng), rmTSLP (100 ng) before analysis 18–24 h after injection. Germ-free C57BL/6 J mice were a gift of the UCSF Gnotobiotic Core Facility. For MC903 experiments, mouse ears were treated with MC903 or ethanol for 5 consecutive days and as previously described[35]. All animal procedures were approved by the University of California San Francisco Institutional Animal Care and Use Committee.

Flow cytometry and cell sorting. Single-cell suspensions from bone marrow (BM), lung, adipose tissue (fat), and small intestinal lamina propria (gut) were prepared are previously described[15,18,36]. For skin single-cell suspensions, pooled ear/back or back tissue was minced in RPMI-1640 with 10% FBS, then transferred to C tubes (Miltenyi Biotec) containing 5 mL of RPMI-1640 supplemented with Collagenase XI (2 mg/mL; Sigma C9407), hyaluronidase (0.5 mg/mL; Sigma H3506), and DNAse I (0.1 mg/mL; Sigma 10104159001). Samples were shaken at 200–250 rpm for 90 min at 37 °C, then dispersed using an automated tissue dissociator (GentleMACS; Miltenyi Biotec) running program C. Single-cell suspensions were passed through a 70-μm filter and washed twice with RPMI containing 10% FBS. The following antibodies, all from BioLegend (unless otherwise specified) were used at 1:100 dilution unless noted: anti-CD3 (17A2), anti-CD4 (RM4–5), anti-CD5 (53–7.3), anti-CD8α (53-6.7), anti-CD11b (M1/70), anti-CD11c (N418), anti-CD19 (6D5), anti-CD25 (PC61), anti-CD44 (IM7), anti-CD45 (30F-11, BD Biosciences), anti-CD49b (DX5; eBiosciences), anti-CD103 (2E7), anti-CD127 (A7R34), anti-CD218 (P3TUNYA, diluted 1:200; eBiosciences), anti-F4/80 (BM8), anti-Gr-1 (RB6–8C5), anti-IL-17RB (9B10, diluted 1:20), anti-NK1.1 (PK136), anti-NKp46 (29A1.4), anti-Thy1.2 (53-2.1; diluted 1:500); anti-human CD4 (RPA-T4, diluted 1:20; eBiosciences), anti-KLRG1 (2F1; eBiosciences), anti-TSLPR (polyclonal; R&D Systems, diluted 1:20), anti-SiglecF (E50–244; BD Biosciences), anti-T1/ST2 (DJ8; MD Biosciences). Live/dead cell exclusion was performed with DAPI (4′,6-diamidine-2′-phenylindole dihydrochloride; Roche). Cell counts were performed using flow cytometry counting beads (CountBright Absolute; Life Technologies) per the manufacturer's instructions.

ILC2s were sorted from reporter mice as live (DAPI⁻), lineage-negative (CD3, CD4, CD8, CD11b, CD11c, CD19, NK1.1, NKp46, Gr-1, F4/80, Ter119, DX5) CD45⁺Red5⁺ for all tissues except for bone marrow (Lin⁻CD45⁺Thy1.2⁺Yarg⁺) and *Crlf2*^{−/−}*Il25*^{−/−}*Il1rl1*^{−/−} small intestine ILC2s (Lin⁻CD45⁺Klrg1⁺Yarg⁺) using a MoFlo XDP (Beckman Coulter). For germ-free mice, ILC2s were sorted as Lin⁻CD45⁺Thy1.2⁺CD25⁺. Sample data were acquired with a five-laser LSRFortessa X-20 flow cytometer and BD FACSDiva software (BD Biosciences) and analyzed using FlowJo software (Tree Star).

RNA preparation and qRT-PCR. ILC2s from various tissues (1,000–10,000 cells per sample) were sorted into RLT Plus lysis buffer (Qiagen) and stored at −80 °C, then processed using RNeasy Micro Plus kit (Qiagen) per the manufacturer's protocol. For qPCR analyses, RNA was reverse transcribed using a SuperScript VILO cDNA synthesis kit (ThermoFisher) and amplified using Power SYBR Green PCR master mix (ThermoFisher) with primers from PrimerBank as listed in Supplementary Table 2.

RNA sequencing. Total RNA was prepared as indicated above, and quality was assessed by Agilent 2100 Bioanalyzer (Agilent Technologies). RNA-sequencing libraries were generated using the Illumina TruSeq stranded mRNA kit, according to the manufacturer's protocol (Illumina). Library concentrations were measured using KAPA Library Quantification Kits (Kapa Biosystems), and equal amounts of indexed libraries were pooled and sequenced on the HiSeq 4000 (Illumina). Sequencing yielded ~6.5 billion reads with a mean read depth of 97.7 million reads/sample. Reads were then aligned to the *Mus musculus* genome, and those that mapped uniquely to known mRNAs were used to assess differential expression. Differential gene expression testing was carried out using DESeq2[37].

DESeq2 was used to carry out pairwise comparisons between tissues with the same genotype and between genotypes in the same tissue. Additionally, DESeq2 was run using a multifactorial model to identify the general effect of each tissue on gene expression (bone marrow was modeled as the intercept), the general effect of the knockout (wild-type as the intercept), and an interaction term between the genotype and the tissue.

For single-cell RNA sequencing (scRNA-seq), ILC2s were sorted as described above into ice-cold 0.5% BSA in PBS and processed through the Chromium Single Cell 3′ v2 Library Kit (10X Genomics) per the manufacturer's protocol. Each channel was loaded with 5,000 to 25,000 cells from each tissue, yielding 400–11,600 single cells for analysis from each tissue. The cells were then partitioned into gel beads in emulsion in the instrument, where cell lysis and barcoded reverse transcription of RNA occurred, followed by amplification, shearing, and 5′-adaptor and sample index attachment. Libraries were sequenced on an Illumina HiSeq 4000. Single Cell 3′ libraries used standard Illumina sequencing primers for both sequencing and index reads and were run using paired-end sequencing with single indexing, in which read 1 was 26 cycles and read 2 was 98 cycles.

The resulting bcl files were demultiplexed using bcl2fastq2.1.7 v, and the resultant paired-end fastq files were aligned to the mm10 transcriptome (ftp://ftp. ensembl.org/pub/release-84/fasta/mus_musculus/dna/Mus_musculus.GRCm38. dna.primary_assembly.fa.gz and ftp://ftp.ensembl.org/pub/release-84/gtf/mus_ musculus/Mus_musculus.GRCm38.84.gtf.gz) using the STAR aligner, which comes packaged in the Cellranger toolkit (version 2.0.0) provided by 10X Genomics. Cellranger aggr was used to aggregate multiple libraries. Details of the pipeline are provided in Supplementary Table 3.

In vitro cell cultures and cytokine quantification. Sorted ILC2s were cultured at 1,500–3,000 cells/well (37 °C, 5% CO2) for 24 h in 100 μL of media containing high glucose (4.5 g/L) DMEM, 10% heat-inactivated FBS, 3.7 g/L NaHCO₃, 0.036 g/L ʟ-asparagine, 0.116 g/L ʟ-arginine, 0.006 g/L folic acid, and supplemented with 10 mM HEPES, pH 7.4, penicillin–streptomycin, and 2-mercaptoethanol (Life Technologies), plus IL-7, IL-18, IL-33, and/or TSLP (all at 10 ng/mL; R&D Systems), or where indicated, ionomycin (500 ng/mL) and phorbol 12-myristate 13-acetate (PMA; 40 ng/mL; Sigma). Cell-free supernatants were collected after centrifugation for protein analysis, while cell pellets were resuspended and stained for flow cytometric analysis. Supernatants were assayed for IL-5 and IL-13 protein amounts using Cytometric Bead Array Flex Sets, acquired with a five-laser LSRFortessa X-20 flow cytometer and BD FACSDiva software, and analyzed using Flow Cytometric Analysis Program (FCAP) Array software (BD Biosciences).

Statistical analysis. Results from independent experiments were pooled whenever possible, and all data were analyzed using Prism 7 (GraphPad Software) by comparison of means using unpaired two-tailed Student's *t* tests. Statistical analysis for RNA-seq data is described above. Data in all figures represent mean ± s.d. unless otherwise indicated.

Accession Codes. All RNA-seq and scRNA-seq data generated in this study are deposited in Gene Expression Omnibus (GEO) under accession code GSE117568.

Reporting Summary. Further information on research design is available in the Nature Research Reporting Summary linked to this article.

Data and code availability statement. The data and software code that support the findings of this study are available from the corresponding author upon reasonable request.

References

35. Li, M. et al. Induction of thymic stromal lymphopoietin expression in keratinocytes is necessary for generating an atopic dermatitis upon application of the active vitamin D3 analogue MC903 on mouse skin. *J. Invest. Dermatol.* **129**, 498–502 (2009).
36. Molofsky, A. B. et al. Innate lymphoid type 2 cells sustain visceral adipose tissue eosinophils and alternatively activated macrophages. *J. Exp. Med.* **210**, 535–549 (2013).
37. Love, M. I., Huber, W. & Anders, S. Moderated estimation of fold change and dispersion for RNA-seq data with DESeq2. *Genome Biol.* **15**, 550 (2014).

nature research

Corresponding author(s):   Richard M. Locksley

Reporting Summary

Nature Research wishes to improve the reproducibility of the work that we publish. This form provides structure for consistency and transparency in reporting. For further information on Nature Research policies, see <u>Authors & Referees</u> and the <u>Editorial Policy Checklist</u>.

Statistical parameters

When statistical analyses are reported, confirm that the following items are present in the relevant location (e.g. figure legend, table legend, main text, or Methods section).

n/a	Confirmed	
☐	☒	The <u>exact sample size</u> (*n*) for each experimental group/condition, given as a discrete number and unit of measurement
☐	☒	An indication of whether measurements were taken from distinct samples or whether the same sample was measured repeatedly
☐	☒	The statistical test(s) used AND whether they are one- or two-sided *Only common tests should be described solely by name; describe more complex techniques in the Methods section.*
☐	☒	A description of all covariates tested
☐	☒	A description of any assumptions or corrections, such as tests of normality and adjustment for multiple comparisons
☐	☒	A full description of the statistics including <u>central tendency</u> (e.g. means) or other basic estimates (e.g. regression coefficient) AND <u>variation</u> (e.g. standard deviation) or associated <u>estimates of uncertainty</u> (e.g. confidence intervals)
☐	☒	For null hypothesis testing, the test statistic (e.g. F, t, r) with confidence intervals, effect sizes, degrees of freedom and P value noted *Give P values as exact values whenever suitable.*
☒	☐	For Bayesian analysis, information on the choice of priors and Markov chain Monte Carlo settings
☐	☒	For hierarchical and complex designs, identification of the appropriate level for tests and full reporting of outcomes
☒	☐	Estimates of effect sizes (e.g. Cohen's *d*, Pearson's *r*), indicating how they were calculated
☐	☒	Clearly defined error bars *State explicitly what error bars represent (e.g. SD, SE, CI)*

Our web collection on <u>statistics for biologists</u> may be useful.

Software and code

Policy information about <u>availability of computer code</u>

Data collection	FACSDiva v8.0.1, StepOne v2.1. For additional details please refer to Methods.
Data analysis	FlowJo vX; Prism v7.0c; Excel v14.5.1; STAR_2.4.2a (Dobin et al., 2013); DESeq2 (Anders and Huber, 2010); CellRanger v2.0 ; Morpheus (https://software.broadinstitute.org/morpheus). For additional details please refer to Methods.

For manuscripts utilizing custom algorithms or software that are central to the research but not yet described in published literature, software must be made available to editors/reviewers upon request. We strongly encourage code deposition in a community repository (e.g. GitHub). See the Nature Research <u>guidelines for submitting code & software</u> for further information.

Data

Policy information about <u>availability of data</u>

All manuscripts must include a <u>data availability statement</u>. This statement should provide the following information, where applicable:
- Accession codes, unique identifiers, or web links for publicly available datasets
- A list of figures that have associated raw data
- A description of any restrictions on data availability

All RNA-seq and scRNA-seq data generated in this study are deposited in Gene Expression Omnibus (GEO) under accession code GSE117568. The data that support the findings of this study are available from the corresponding author upon reasonable request.

Field-specific reporting

Please select the best fit for your research. If you are not sure, read the appropriate sections before making your selection.

☒ Life sciences ☐ Behavioural & social sciences ☐ Ecological, evolutionary & environmental sciences

For a reference copy of the document with all sections, see nature.com/authors/policies/ReportingSummary-flat.pdf

Life sciences study design

All studies must disclose on these points even when the disclosure is negative.

Sample size	No statistical methods were used to predetermine sample size. At minimum of 3 individual mice were used for all the experiments and assumed this would be required to recognize differences between genotypes or conditions. Additional details for each figure panel is included in the figure legends.
Data exclusions	No data was excluded.
Replication	Experiments were replicated at least twice as described throughout the paper and in the Methods.
Randomization	Mice of similar ages and sex were used for all the experiments reported. Samples were randomly assigned.
Blinding	The investigators were not blinded to the identities of the samples because treatments and data collection were performed by the same people. All samples were collected and analyzed at the same time under the same conditions.

Reporting for specific materials, systems and methods

Materials & experimental systems

n/a	Involved in the study
☐	☒ Unique biological materials
☐	☒ Antibodies
☒	☐ Eukaryotic cell lines
☒	☐ Palaeontology
☐	☒ Animals and other organisms
☒	☐ Human research participants

Methods

n/a	Involved in the study
☒	☐ ChIP-seq
☐	☒ Flow cytometry
☒	☐ MRI-based neuroimaging

Unique biological materials

Policy information about availability of materials

Obtaining unique materials	Red5 (IL-5-tdTomato) reporter mice are available upon reasonable request. Smart 13 (IL-13-huCD4) reporter mice (Stock No. 018869) and Yarg (Arg1-YFP) reporter mice (Stock No. 015857) are available at Jackson Laboratories.

Antibodies

Antibodies used	The following antibodies, all from BioLegend and various Lot #s (unless otherwise specified) were used at 1:100 dilution unless noted: anti-CD3 (Clone 17A2, PE/Cy7 Cat No. 100220), anti-CD4 (Clone RM4-5, BV605 Cat No. 100548, BV711 Cat No. 100548), anti-CD5 (Clone 53-7.3, BV421 Cat No. 100629), anti-CD8α (Clone 53-6.7, BV421 Cat No. 100753, BV785 Cat. No100750), anti-CD11b (Clone M1/70, BV650 Cat No. 101259, AF647 Cat No. 101218), anti-CD11c (Clone N418, BV785 Cat No. 117336, PE/Cy7 Cat No. 117318), anti-CD19 (Clone 6D5, BV421 Cat No. 115538), anti-CD25 (Clone PC61, APC/Fire750 Cat No. 102054), anti-CD44 (Clone IM7, BV711 Cat No. 103057, BV785 Cat No. 103059), anti-CD45 (Clone 30F-11, BD Biosciences, BV711 Cat No. 564357, UV395 Cat No 564279), anti-CD49b (Clone DX5, eBiosciences, eF450 Cat No. 48-5971), anti-CD103 (Clone 2E7, PerCP/Cy5.5 Cat No. 121416), anti-CD127 (Clone A7R34, BV605 Cat No. 135025), anti-CD218 (Clone P3TUNYA, diluted 1:200, eBiosciences, PerCP-eF710 Cat No. 46-5183-82), anti-F4/80 (Clone BM8, PB Cat No. 123124), anti-Gr-1 (Clone RB6-8C5, PB Cat No. 108430), anti-IL-17RB (Clone 9B10, diluted 1:20, APC Cat No. 146308), anti-NK1.1 (Clone PK136, PB Cat No. 108722), anti-NKp46 (Clone 29A1.4, PB Cat No. 331912), anti-Thy1.2 (Clone 53-2.1, diluted 1:500, BV605 Cat No. 140318); anti-human CD4 (Clone RPA-T4, diluted 1:20; eBiosciences, APC, Cat No. 17-0049), anti-KLRG1 (Clone 2F1, eBiosciences, PerCP-eF710 Cat No. 46-5893-82), anti-TSLPR (polyclonal, R&D Systems, diluted 1:20, APC Cat No. FAB5461A), anti-SiglecF (Clone E50-244, BD Biosciences, AF647 Cat No 562680), anti-T1/ST2 (Clone DJ8; MD Biosciences, FITC Cat No. 101001).

Validation	All the antibodies used have undergone extensive validation by the manufacturer.

Animals and other organisms

Policy information about [studies involving animals](); [ARRIVE guidelines]() recommended for reporting animal research

Laboratory animals	Il5Red5, Arg1Yarg, and Il13Smart reporter alleles on wild-type and triple-deficient Crlf2−/−Il25−/−Il1rl1−/− C57BL/6J backgrounds were bred and maintained as described previously. Il18−/− mice were obtained from The Jackson Laboratory (Stock 004130). Germ-free animals were provided by the UCSF Gnotobiotic Mouse Facility. For all experiments, age-(7-14 weeks) and sex-matched animals were used. All animal procedures were approved by the University of California San Francisco Institutional Animal Care and Use Committee.
Wild animals	This study did not involve wild animals.
Field-collected samples	The study did not involve samples collected from the field.

Flow Cytometry

Plots

Confirm that:

☒ The axis labels state the marker and fluorochrome used (e.g. CD4-FITC).

☒ The axis scales are clearly visible. Include numbers along axes only for bottom left plot of group (a 'group' is an analysis of identical markers).

☒ All plots are contour plots with outliers or pseudocolor plots.

☒ A numerical value for number of cells or percentage (with statistics) is provided.

Methodology

Sample preparation	See Methods, "Flow Cytometry and Cell Sorting"
Instrument	Becton Dickinson 5-laser LSRFortessa X-20 flow cytometer for analysis and MoFlo XDP (Beckman Coulter) for cell sorting.
Software	BD FACSDiva software (BD Biosciences) for data acquisition and analyzed using FlowJo software version X (Tree Star). Data was graphed using Prism 7 (Graphpad).
Cell population abundance	The purities of sorted cell populations were consistently > 98%.
Gating strategy	The gating strategy is shown in Extended Data Figure 1.

☒ Tick this box to confirm that a figure exemplifying the gating strategy is provided in the Supplementary Information.